IVYSPRING INTERNATIONAL PUBLISHER

Theranostics

2017; 7(3): 775-788. doi: 10.7150/thno.17237

Research Paper

Liposomal Nanoparticles Carrying anti-IL6R Antibody to the Tumour Microenvironment Inhibit Metastasis in Two Molecular Subtypes of Breast Cancer Mouse Models

Chunlei Guo[1*], Yanan Chen[1*], Wenjuan Gao[1], Antao Chang[1], Yujie Ye[1], Wenzhi Shen[1], Yunping Luo[2], Shengyong Yang[3], Peiqing Sun[4], Rong Xiang[1,5,6]✉, and Na Li[1,5,6]✉

1. School of Medicine, Nankai University, 94 Weijin Road, Tianjin 300071, China;
2. Department of Immunology, Institute of Basic Medical Science, Peking Union Medical College, Beijing 100730, China;
3. State Key Laboratory of Biotherapy and Cancer Center, Sichuan University, Chengdu 610041, China.
4. Department of Cancer Biology, Wake Forest University School of Medicine, Winston-Salem, NC 27157, USA.
5. Tianjin Key Laboratory of Tumour Microenvironment and Neurovascular Regulation, Tianjin 300071, China.
6. Collaborative Innovation Center for Biotherapy, Nankai University, 94 Weijin Road, Tianjin 300071, China.

* Chunlei Guo and Yanan Chen contributed equally to this paper.

✉ Corresponding authors: Dr. Na Li, Tel. (86)-22-23509482; Email: lina08@nankai.edu.cn and Dr. Rong Xiang, Tel. (86)-22-23509482; Email: rxiang@nankai.edu.cn.

Received: 2016.08.17; Accepted: 2016.12.04; Published: 2017.01.26

Abstract

Tumour microenvironment (TME) contributes significantly towards potentiating the stemness and metastasis properties of cancer cells. IL6-Stat3 is one of the important cell signaling pathways in mediating the communication between tumour and immune cells. Here, we have systematically developed a novel anti-CD44 antibody-mediated liposomal nanoparticle delivery system loaded with anti-IL6R antibody, which could specifically target the TME of $CD44^+$ breast cancer cells in different mouse models for triple negative and luminal breast cancer. This nanoparticle had an enhanced and specific tumour targeting efficacy with dramatic anti-tumour metastasis effects in syngeneic BALB/c mice bearing 4T1 cells as was in the syngeneic MMTV-PyMT mice. It inhibited IL6R-Stat3 signaling and moderated the TME, characterized by the reduced expression of genes encoding Stat3, Sox2, VEGFA, MMP-9 and CD206 in the breast tissues. Furthermore, this nanoparticle reduced the subgroups of $Sox2^+$ and $CD206^+$ cells in the lung metastatic foci, demonstrating its inhibitory effect on the lung metastatic niche for breast cancer stem cells. Taken together, the CD44 targeted liposomal nanoparticles encapsulating anti-IL6R antibody achieved a significant effect to inhibit the metastasis of breast cancer in different molecular subtypes of breast cancer mouse models. Our results shed light on the application of nanoparticle mediated cancer immune-therapy through targeting TME.

Key words: liposomal nanoparticles, anti-IL6R antibody, tumour microenvironment, metastasis, metastatic niche.

Introduction

Breast cancer is among the high-morbidity malignant tumours worldwide and is now the second leading lethal tumour type for women [1]. Although the improvement in early detection and therapeutic method may improve the survival times, many breast cancer patients still succumb to this disease due to tumour metastasis [2].

Nanoparticles (NPs) have been widely explored for the delivery of anticancer drugs to tumour sites [3, 4]. The central aim of delivery systems is to accumulate the loading drugs efficiently at target sites in their bioavailable forms [5-7]. Liposomal

nanoparticles have been widely investigated because of their fine biological properties such as low immunogenicity, good biocompatibility, biodegradability, and the ability to hold a large payload of hydrophilic and hydrophobic agents since they possess both hydrophobic membrane and aqueous reservoir. Inclusion of the PEGylated lipids in liposomes was developed as one of clinically suitable liposome formulations since they protected liposomes from the destruction by reticulo-endothelial system (RES), thus increased the circulation time and drug accumulation in tumours, resulting in the enhanced antitumour efficacy [8, 9]. Once localized in the tumour tissues, the loading drug should be released at a proper rate so that it can reach the target cells at an effective therapeutic concentration. To trigger the release of drug in tumour site specifically, a variety of liposomes were designed which could response to the changes in pH [10, 11], temperature [12], enzymes [13], light [14] and magnetic pulses [15]. Among them, pH-responsive liposome was most commonly used, regarding that there is a tremendous variation for the pH values in different tissues and cellular compartments. In addition to relying solely on passive targeting, nanoparticles were frequently modified with targeting ligands for the specific reorganization of receptors which is overexpressed or present on tumour cells membrane.

CD44 is a multifunctional and widely distributed cell surface glycoprotein. It has been identified as one of the most established biomarkers for cancer stem cells (CSCs), which show chemo-resistant and highly malignant properties in numerous types of tumours, including breast, prostate, colon and pancreatic cancers etc. [16-18]. For tumour-site-specific delivery of anticancer drugs, anti-CD44 monoclonal antibody (mAb) can be coupled to the surface of liposomes**,** targeting $CD44^+$ cancer cells [19]. CSCs play important roles in initiation and relapse of cancers due to their self-renewal and pluripotency properties**.** They are resistant to most of the cytotoxic agents [20]. Thus, CSCs were thought to be a vital source for tumour recurrence and metastasis. Consequently, with the aim of eliminating CSCs, the targeted drug delivery strategy is an ideal approach to increase the efficacy of anticancer therapy [20]. However, development of effective means to deliver the therapeutics to CSCs specifically is one of the most formidable challenges.

Tumour tissues are composed of tumour cells and non-tumour cells, which include macrophages, endothelial cells, fibroblasts, pericytes, innate and adaptive immune cells, mesenchymal cells, etc. [21]. The interactions between non-tumour and tumour cells thus form tumour microenvironment (TME). Cancer cells and CSCs educate the surrounding cells to form an immune-favourable microenvironment through releasing extracellular signals. The non-tumour cells in turn promotes the development of cancer by boosting the stemness, metastasis and chemo-resistant properties of cancer cells [22]. Moreover, non-tumour cells and cancer cells secrete a variety of chemokines and cytokines to activate and mobilize the stromal cells (e.g., macrophages, bone marrow progenitor cells) to form pre-metastatic niches in the distant organs, such as lungs, etc., to promote the survival of metastatic tumour cells [23, 24]. Thus, targeting the communication between the non-tumour cells and cancer cells as well as CSCs in TME is a promising strategy in tumour therapy. Interleukin-6, an inflammatory cytokine, binds to its receptor IL6R-IL6ST (GP130) to activate Janus kinases (JAK), which subsequently phosphorylates and activates its downstream target- signal transducer and activator of transcriptions (STATs), including STAT3, to regulate the expression of VEGF and matrix metalloproteinases (MMPs, e.g. MMP-2 and MMP-9) etc.[25, 26]. This enhances the migration and invasion of tumour cells [27]. In addition, IL6-STAT3 signaling was reported to maintain the properties of CSCs [28, 29]. Higher expression levels of IL6 receptor α (IL6Rα) and gp130 were detected in CSCs than in non-CSCs, and targeting of IL-6 ligand or IL6Rα in glioma stem cells significantly reduced the growth and sphere-formation capacity [30]. Moreover, IL-6 promotes the polarization of macrophages from M1 to M2 phenotype [31], which plays a vital role in promoting the stemness and enhancing the metastasis properties of cancer cells in the TME [32, 33]. Based on this knowledge, development of a delivery system that can specifically target the IL6R-STAT3 signaling may effectively block the communication between cancer cells and the TME, thus inhibit the development of cancer.

Our previous study demonstrated the abundance of tumour associated macrophages (TAMs, M2 phenotype) in breast tumour tissues and the recruitment effect of CSCs marker protein-Sox2 on TAMs [33]. This study aimed to develop CD44 targeted liposomal nanoparticles for the triggered release of their encapsulated contents into the extracellular matrix. Here, we developed a novel anti-CD44 antibody-mediated liposomal nanoparticle loaded with anti-IL6R antibody. This delivery system specifically targeted the TME of $CD44^+$ breast cancer cells in 4T1 tumour-bearing mice and MMTV-PyMT mice, in which CD44 was expressed. We found that this nanoparticle blocked the IL6R signaling in cancer cells as well as the macrophages, thus suppressed the stemness, metastasis and angiogenesis of breast

cancer. Furthermore, it modified the lung metastatic foci by reducing the amount of M2 macrophages, which may lead to the decreased number of metastatic $Sox2^+$ cancer cells. Our study provided exciting explorations in applying immune-interference therapy to breast cancer by using the TME targeting nanoparticle.

Materials and methods

Cell line and cell culture

The 4T1 mouse mammary tumour cell line was cultured in the RPMI-1640 medium supplemented with 10% fetal bovine serum, 100 units/mL penicillin and 100 μg/mL streptomycin. The cells were incubated at 37 °C in the presence of 5% CO_2.

Preparation of liposomal nanoparticles (NPs)

The liposomes were composed of 1,2-dioleoyl-sn-glycero-3-phosphocholine (DOPC), 1,2-dioleoyl-sn-glycero-3-phosphoethanolamine (DOPE), cholesterol (Avanti Polar Lipids Inc., Alabaster, AL, USA) and 1,2-distearoyl-sn-glycero-3-phosphoethanolamine-N-[succinimidyl(polyethylene glycol)-3400] (DSPE–PEG_{3400}–NHS, Nanocs Inc., New York, NY, USA). To form the liposomes, a lipid mixture composed of DOPC, DOPE and cholesterol (1:1:1 molar ratio) was prepared in chloroform and added into a glass flask. The chloroform solvent was then evaporated at room temperature and a thin lipid film formed. To remove residual chloroform from the lipid film completely, the flask was dried for 12 hours (hs). The dried lipids were rehydrated in phosphate buffered saline (PBS, pH 7.4, 10 mM Na_2HPO_4, 1.76 mM KH_2PO_4, 137 mM NaCl, 2.7 mM KCl). The suspension was then forced through two polycarbonate filters with 100 nm pores using the Nuclepore Track-Etch Membrane (Whatman, Maidstone, UK). The prepared liposome was then stored at 4 °C until use.

For preparation of per 1 mL of the liposomal nanoparticles or CD44 targeted liposomal nanoparticles encapsulating anti-IL6R antibody (NPs-αIL6R Ab or NPs-αIL6R Ab-CD44), 20 μg of the anti-IL6R antibody (Santa Cruz Biotechnology, Dallas, Texas, USA) was dissolved in 1 mL of PBS at 4°C for 5 min before pipetting it to the flask containing 1 mL of lipid films. For fully hydration purpose, the mixture was put into the rotary evaporator for 1 h [34]. And then, the mixture was extruded 10 times through a mini-extruder equipped with 100 nm polycarbonate membrane filter to form liposomal NPs of a predetermined diameter. After encapsulation, to remove the non-encapsulated antibody, the free antibody was separated by size exclusion chromatography system (GE Healthcare, USA), which was equipped with a XK 16/40 column packed with Bio-Gel 15M resin (Bio-Rad, Hercules, CA, USA) by using PBS (pH 7.4) as the running buffer [34]. The CD44 targeted liposomes were prepared through a modified post-insertion method (**Fig. 1A**). Briefly, DSPE-PEG_{3400}-NHS was mixed with the monoclonal anti-CD44 antibody (BD Bioscience, San Jose. CA) at a molar ratio of 10:1 (micelle/antibody). The amine of anti-CD44 antibody bound to end-functionalized groups of PEG in preformed micelles via ester conjugation [35]. And then, CD44-PEG conjugates were mixed with liposomes at a 1:100 molar ratio for 4-8 hs with continuous stirring.

The procedure for preparing the CD44 targeted liposomal nanoparticles loaded with doxorubicin (Dox, a red-coloured antibiotic, 1mg/1mL lipid) (Sigma-Aldrich Corp., St. Louis, MO, USA) or IgG (20 μg/1mL lipid) (abcam, Cambridge, UK) was similar to that for NPs-αIL6R Ab-CD44.

Characterization of the NPs

The particle size and polydispersity index of liposomes were measured by dynamic light scattering, and zeta-potential was determined by phase analysis light scattering (Zeta PALS, Brookhaven Instruments, Holtsville, NY, USA). The solution containing liposomal NPs was dropped onto a copper mesh and then negatively stained with 2% (weight/volume) uranyl acetate. After 1 h's drying, the morphology of the sample was observed under a Philips CM200 transmission electron microscope (TEM), which was operated at an acceleration voltage of 80 kV.

Drug loading and encapsulation efficiency for NPs and the *in vitro* drug release

The amount of free drugs presented in the supernatant or dialysis were measured by GloMax®-Multi Detection System (Promega). They were determined through measuring the absorbance at 480 nm using ultraviolet-visible (UV-Vis) spectrophotometry (for Dox) and the fluorescence intensity value at excitation of 490 nm and emission of 510-570 nm using fluorescence spectrophotometry (for anti-IL6R Ab-PE), then were calculated based on their corresponding calibration curves separately.

Drug loading and encapsulation efficiency experiments were performed in triplicate by determining the amount of Dox as well as anti-IL6R Ab-PE (αIL6R Ab-PE, BD Biosciences, San Jose, CA, USA) presented in the supernatants during preparation. The mass (*M*) of the Dox- or anti-IL6R Ab-PE loaded nanoparticles was weighed after being dried under vacuum overnight at 4 °C. Drug

encapsulation efficiency and loading efficiency were then determined by using the following formulas: Encapsulation efficiency (%) = *M* (feeding drug) – *M* (drug in supernatant) / *M* (feeding drug) × 100%; Drug loading efficiency (%) = *M* (feeding drug) – *M* (drug in supernatant) / *M* (the weight of nanoparticles) × 100% [36].

To assess the release behavior of Dox and anti-IL6R Ab-PE under different pH conditions, 3 mL of Dox or anti-IL6R Ab-PE loaded nanoparticles were placed into a dialysis bag, which was placed in a reservoir containing 150 mL of PBS (pH = 7.4, 6.5, 5.0, respectively), stirred at 100 rpm at 37 ℃. 1-mL dialysate was removed from the sample at proper intervals, followed by storage at -20 ℃ for the later analyses. To keep a constant volume, 1 mL of fresh PBS with corresponding pH was added to the reservoir at each sampling time [36].

Tumour xenograft mouse model and assay of the bio-distribution of drug in mice treated with CD44 targeted NPs

All of the *in vivo* mice experiments were approved by the Nankai University Animal Care and Use Committee. 6-8 week-old syngeneic BALB/c female mice were separated randomly into four groups. 5×10^4 4T1 cells were injected into the fourth right mammary fat pad of each mouse. The tumour-bearing mice were injected with NPs-Dox (5 mg/kg body weight (BW) of Dox), NPs-Dox-CD44 (5 mg/kg BW of Dox), NPs-αIL6R Ab-PE (200 μg / kg BW of Ab) or NPs-αIL6R Ab-PE-CD44 (200 μg / kg BW of Ab) via tail vein on the 10th day after graft. Syngeneic MMTV-PyMT female mice were injected with above nanoparticles at same dose via tail vein after 4 weeks of tumorigenesis. The mice were sacrificed 4 hs (for NPs-Dox and NPs-Dox-CD44 treatment group) after injection to avoid the toxic effect of Dox to the organs [19] and 6 hs for NPs-αIL6R Ab-PE and NPs-αIL6R Ab-PE-CD44 treatment group after injection. Various major tissues or organs including the tumour, heart, liver, spleen, lung, kidney, brain and intestine were removed for the detection of the bio-distribution and concentration of Dox or αIL6R Ab-PE in them. Similar volume of tissue slice from each corresponding organ was dissolved and homogenized in PBS (PH 7.4). To determine the concentration of Dox in the tissues, 100 μL of 1% sodium dodecyl sulfate and 100 μL of 1mM H_2SO_4 were added to 1mL of tissue homogenate. Then, Dox was extracted through adding 2 mL of isopropyl alcohol/chloroform (1:1, volume ratio) to the homogenized samples, followed by vortex and three rounds of freeze/thaw cycles. The samples were centrifuged at 14,000 g for 15 minutes and the organic phase which presented in the lower phase was measured. To measure the concentration of αIL6R Ab-PE, tissue was homogenized in 500 uL PBS. They were measured directly by using GloMax®-Multi Detection System (Promega).

Application of NPs in different mouse models.

The syngeneic mice were randomly separated into five groups and injected with PBS, anti-IL6R Ab, NPs-IgG-CD44, NPs-αIL6R Ab or NPs-αIL6R Ab-CD44 (10 mL/kg BW of PBS, 200 μg /kg BW of Ab or IgG) through the tail vein after tumorigenesis. For the mice grafted with 4T1, tail vein injections were carried out on day 10, 12 and 14 after the graft, respectively. For MMTV-PyMT mice, tail vein injections were carried out on day 6, 8 and 10 after the tumorigenesis, respectively. One sporadic tumour from each mouse with similar size to those of other mice was monitored. Its volume was measured till 30 days after tumorigenesis before its amalgamation with neighbour spontaneous tumour(s). The tumour size was measured by using a calliper, the tumour volumes were calculated by using the formula (length × width^2/2). Lung metastatic foci number was determined from all five lobes for each mouse. The percentage of lung metastatic foci area for each mouse was calculated as the area of metastatic foci versus the total area of five lobes in the tissue slices by using the Photoshop software (Adobe, San Jose, CA, USA). Each mouse was injected with 1mg BrdU intraperitoneally 24 hs before the sacrifice as described before [37].

Immunofluorescence staining

The frozen sections were fixed in cold methanol for 15 minutes and then incubated with anti-BrdU, anti-Sox2 (abcam, Cambridge, UK), anti-CD44, anti-F4/80 (BD Biosciences, San Jose, CA, USA), anti-Rab5 or anti-Rab7 (Cell Signaling Technology, Danvers, MA, USA) antibody overnight at 4 ℃, followed by incubation with Alexa Fluor 488 goat anti-rat IgG, Alexa Fluor 488 goat anti-rabbit IgG or Alexa Fluor 594 goat anti-rat IgG, correspondingly (Molecular Probes, Eugene, OR, USA) at room temperature for 1 h. They were finally incubated with DAPI (4',6-diamidino-2-phenylindole, Sigma-Aldrich, St. Louis, MO, USA) for nuclear counterstaining. Images were acquired by using a laser scanning confocal microscope (Leica, Wetzlar, Germany). The red fluorescence of Dox and αIL6R Ab-PE in the tumour tissue was also imaged by using the confocal microscopy at the excitation and emission wavelengths of 488 nm and 594 nm, respectively.

Immunohistochemistry staining

Immunohistochemistry staining was performed

on the tumour and lung tissues of BALB/c mice as well as MMTV-PyMT mice by using antibody against Stat3, p-Stat3 (Santa Cruz Biotechnology, Dallas, Texas, USA), MMP-9, CD31, Sox2, CD206 (abcam, Cambridge, UK), VEGFA (Proteintech, Wuhan, China) separately, followed by standard streptavidin–biotin method by using the 3,3′-Diaminobenzidine (DAB) substrate. The images were recorded by an Olympus BX51 Epi-fluorescent microscope (Olympus Co. Tokyo, Japan). The *H*-score for each protein incorporates staining intensity (negative, weak, moderate and strong were graded as 0, 1, 2, 3 separately) multiplied by the percentage of cells that stained positive based on the images observed under a 10× objective.

Statistical analysis

Student's *t*-test was used to perform the statistical analysis. A p-value < 0.05 was considered statistically significant. Statistical significance is indicated as the following: * indicates $p < 0.05$; and ** indicates $p < 0.01$.

Results

Characterization of CD44 targeted liposomal nanoparticles.

The procedure for the preparation of CD44 targeted liposomal nanoparticles encapsulating anti-IL6R antibody (NPs-αIL6R Ab-CD44) or Doxorubicin (NPs-Dox-CD44) was summarized in **Figure 1A**. The schematic diagram showing the release of cargo drugs to TME of CD44$^+$ breast cancer cells by the CD44 targeted liposomal nanoparticles was described in **Figure 1B** and **1C**. In addition, the particles were spherical and approximately 100 nm in size as revealed by transmission electron microscopy (TEM) in **Figure 2A**. Meanwhile, the dynamic light scattering (DLS) measurements showed that the mean diameter of NPs was ~100 nm (**Figure 2B** and **Figure S1**), which were in accordance with the TEM observations. Furthermore, the polydispersity index (PDI), which reflects the particle size distribution, was narrow for each of these eight nanoparticles (**Figure 2C**).

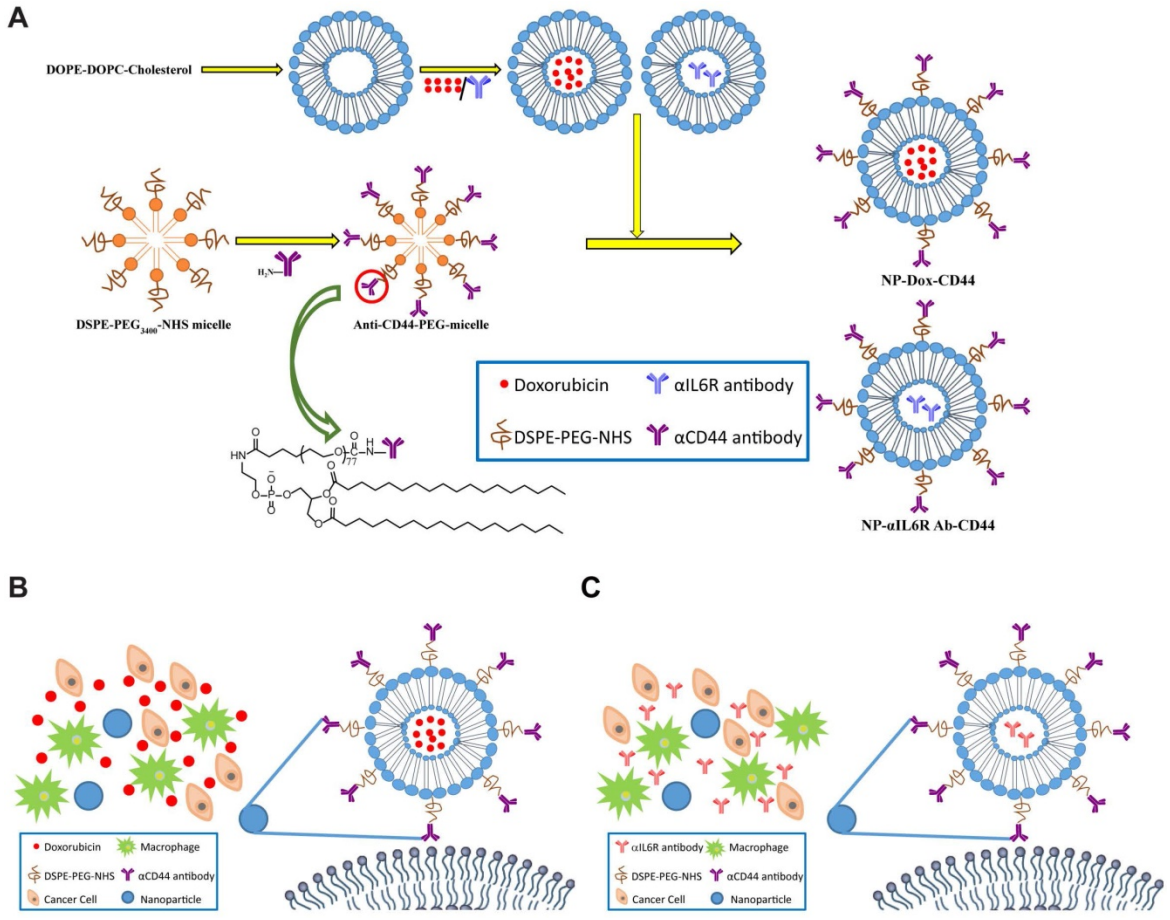

Figure 1. Schematic diagram of the liposomal nanoparticles. **A.** Diagrammatic sketch to show the preparation of NPs-Dox-CD44 and NPs-αIL6R Ab-CD44. Schematic diagram of CD44-targeted liposomes loaded with Dox (**B**) or anti-IL6R antibody (**C**) presented in the TME. The skeleton was a phospholipid bilayer with Dox or anti-IL6R antibody being encapsulated.

Drug encapsulation efficiency, loading efficiency and release *in vitro*

The quality of the liposomal nanoparticles as a drug carrier was evaluated by the encapsulation efficiency of Dox and anti-IL6R Ab-PE as well as their loading efficiency. The encapsulation efficiencies of NPs-Dox, NPs-Dox-CD44, NPs-αIL6R Ab-PE and NPs-αIL6R Ab-PE-CD44 were 85.81 ± 0.4799%, 85.47 ± 0.6729%, 87.01 ± 1.668%, 89.03 ± 1.143%, respectively. The drug loading efficiencies of NPs-Dox and NPs-Dox-CD44 were 12.27 ± 0.3882%, 12.93 ± 0.6855%, respectively (**Figure 2D**). From these results, we can deduce that the liposomal nanoparticles described here have high encapsulation efficiency and drug loading content.

The release profiles of Dox and anti-IL6R Ab-PE from NPs under different pH conditions were measured to evaluate the effects of pH on drug unloading. As shown in **Figure 2E** and **2F**, each release profile was represented by the percentage of released Dox or anti-IL6R Ab-PE as a function of time. We found that the amount of Dox and anti-IL6R Ab-PE released from the CD44 targeted and non-targeted NPs was pH dependent. In neutral environment (pH 7.4), only ~33% of Dox and ~39% of anti-IL6R Ab-PE were released within 48 hs. By contrast, ~77% of Dox and ~68% of anti-IL6R Ab-PE were released within 48 hs at pH 6.5 medium for both NP systems. As we know that the extracellular microenvironments of tumour cells are acidic, the pH values of intracellular endosomes and lysosomes are even lower. At pH 5.0 condition, ~92% of Dox and ~88% of anti-IL6R Ab-PE were released from both NP systems within 48 hs. The results indicated that the release of Dox and anti-IL6R Ab-PE from the liposomal nanoparticles speeded up with the decrease of pH value. Taken together, the pH-sensitive nanoparticle delivery system may potentially facilitate active drug accumulation in tumour tissues and improve specific drug delivery as well as reduce the toxicity to normal tissues.

Enriched bio-distribution of CD44 targeted liposomes in tumour tissues of triple negative and luminal breast cancer mouse models *in vivo*

The distribution and accumulation of administered drugs in main organs and tumours could directly affect their therapeutic efficiency and lead to side effects. To test the efficacy of CD44 targeted liposomes *in vivo*, we administered CD44 targeted nanoparticles encapsulating anti-IL6R Ab-PE or Dox via the tail vein into mice bearing 4T1 breast tumour, which are triple negative and possess mesenchymal and high metastatic properties[38, 39], non-targeted nanoparticles encapsulating anti-IL6R Ab-PE or Dox were administered as the control. The bio-distribution of anti-IL6R Ab-PE or Dox in each tissue was observed by confocal microscopy and was quantified by spectrophotometric measurements. As a result, when compared with the control, CD44 targeted NPs treatment group had more than 6-fold accumulation of anti-IL6R Ab-PE (**Figure 3A** and **3B**) and more than 4-fold accumulation of Dox in 4T1 tumour xenografts (**Figure S2A** and **S2B**), but the accumulation of anti-IL6R Ab-PE in the non-targeting organs such as heart, liver, spleen, lung, kidney and intestine reduced (**Figure 3A** and **3B**). Similarly, the accumulation of Dox in the liver, spleen, kidney and intestine decreased (**Figure S2A** and **S2B**).

The nanoparticles were also applied to MMTV-PyMT mice, which were reported to develop spontaneous and multi-focal cancers of the mammary glands with short latency at 100% incident rate and develop metastatic disease at > 85 % incident rate [40]. They showed similar gene-expression profiles to human luminal breast cancer [41], thus represented a model of luminal breast cancer with a high metastatic potential.

We found that anti-IL6R Ab-PE had 11-fold greater accumulation in tumours compared to the control in MMTV-PyMT mice and the accumulation reduced in the non-targeted organs such as liver, spleen, lung, kidney and intestine (**Figure 3E** and **3F**). Similarly, enrichment of Dox in tumour tissues and lower accumulation in the main organs (heart, liver, spleen, kidney and intestine) were also observed in MMTV-PyMT mice treated with NPs-Dox-CD44 when compared with the NPs-Dox treatment control (**Figure S2E** and **S2F**). Immunofluorescent staining results showed that besides some accumulations in the cell, anti-IL6R Ab-PE and Dox were mainly released into the extracellular matrix of $CD44^+$ tumour cells (**Figure 3C** and **3G**, **Figure S2C** and **S2G**) and might also interact with surrounding macrophages ($F4/80^+$) in the TME (**Figure 3D** and **3H**, **Figure S2D** and **S2H**). In addition, tumour cells co-expressing CD44 and Sox2, which were the CSCs markers, were found in tumour tissues (**Figure S3A**).

These results demonstrated that our liposomal nanoparticles could deliver the cargo to cancer cells, as well as CSCs and macrophages in TME. Furthermore, they were more efficient in delivering drugs to solid tumours than the non-targeted liposome. At the same time, the drug concentrations in non-targeted organs and tissues were reduced, indicating that the systemic side effects of this nanoparticle were minimized.

A

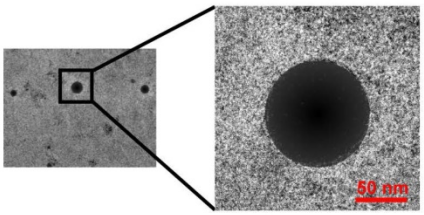

B

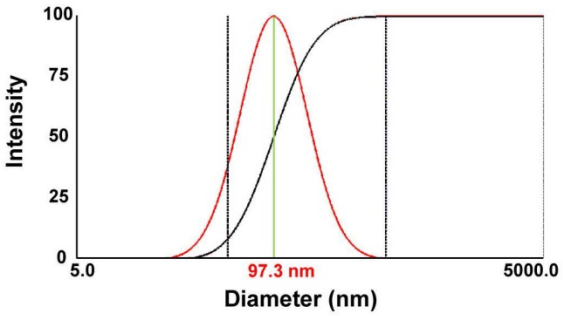

C

Liposomes	Size (nm)	Polydispersity index	Zeta potential (mV)
NPs	92.1 ± 1.0	0.136 ± 0.012	-25.82 ± 4.02
NPs-Dox	96.7 ± 2.3	0.258 ± 0.014	-22.61 ± 2.36
NPs-Dox-CD44	111.4 ± 2.5	0.195 ± 0.011	-17.58 ± 1.82
NPs-IgG-CD44	121.1 ± 1.9	0.213 ± 0.015	-10.62 ± 2.25
NPs-αIL6R Ab	102.8 ± 2.1	0.180 ± 0.007	-23.75 ± 1.58
NPs-αIL6R Ab-CD44	114.6 ± 1.6	0.184 ± 0.011	-14.26 ± 2.51
NPs-αIL6R Ab-PE	96.2 ± 5.1	0.241 ± 0.010	-22.55 ± 2.33
NPs-αIL6R Ab-PE-CD44	119.0 ± 2.4	0.165 ± 0.005	-10.16 ± 1.93

D

Liposomes	Encapsulation efficiency %	Drug loading efficiency %	Drug loading quantity (μg/mL)
NPs-Dox	85.81 ± 0.4799	12.27 ± 0.3882	--
NPs-Dox-CD44	85.47 ± 0.6729	12.93 ± 0.6855	--
NPs-αIL6R Ab-PE	87.01 ± 1.6680	--	17.40 ± 0.3336
NPs-αIL6R Ab-PE-CD44	89.03 ± 1.1430	--	17.81 ± 0.2286

E

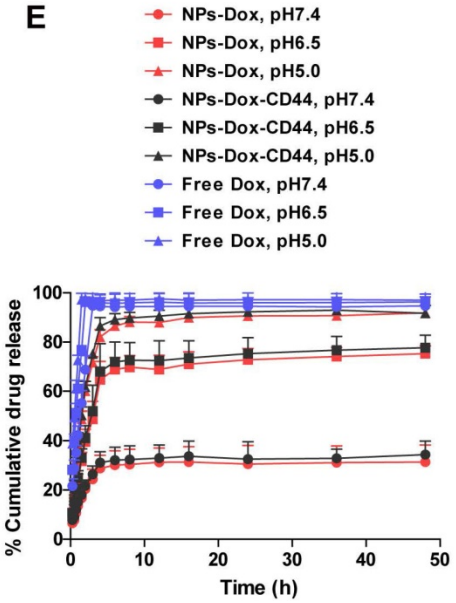

F

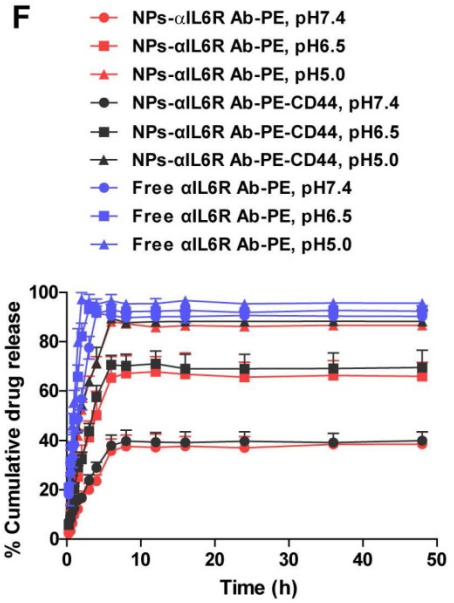

Figure 2. Characterization of CD44 targeted liposomal nanoparticles. **A.** The TEM image of NPs-Dox. The diameter was approximately 100 nm and the sizes of the nanoparticles were uniform. **B.** Representative DLS measurement for size distribution of NPs-Dox. **C.** The characterizations of the eight nanoparticles. Data were presented as the mean ± **standard error of the mean (SEM, n = 3)**. **D**. The encapsulation efficiency, drug loading efficiency or quantity of Dox and anti-IL6R Ab-PE in the liposomal nanoparticles. Data were presented as the mean ± standard deviation (SD, n = 4). *In vitro* release profiles of Dox (**E**) and anti-IL6R Ab-PE (αIL6R Ab-PE, **F**) from nanoparticles under different pH values at 37°C. Data were presented as the mean + SD, n = 4.

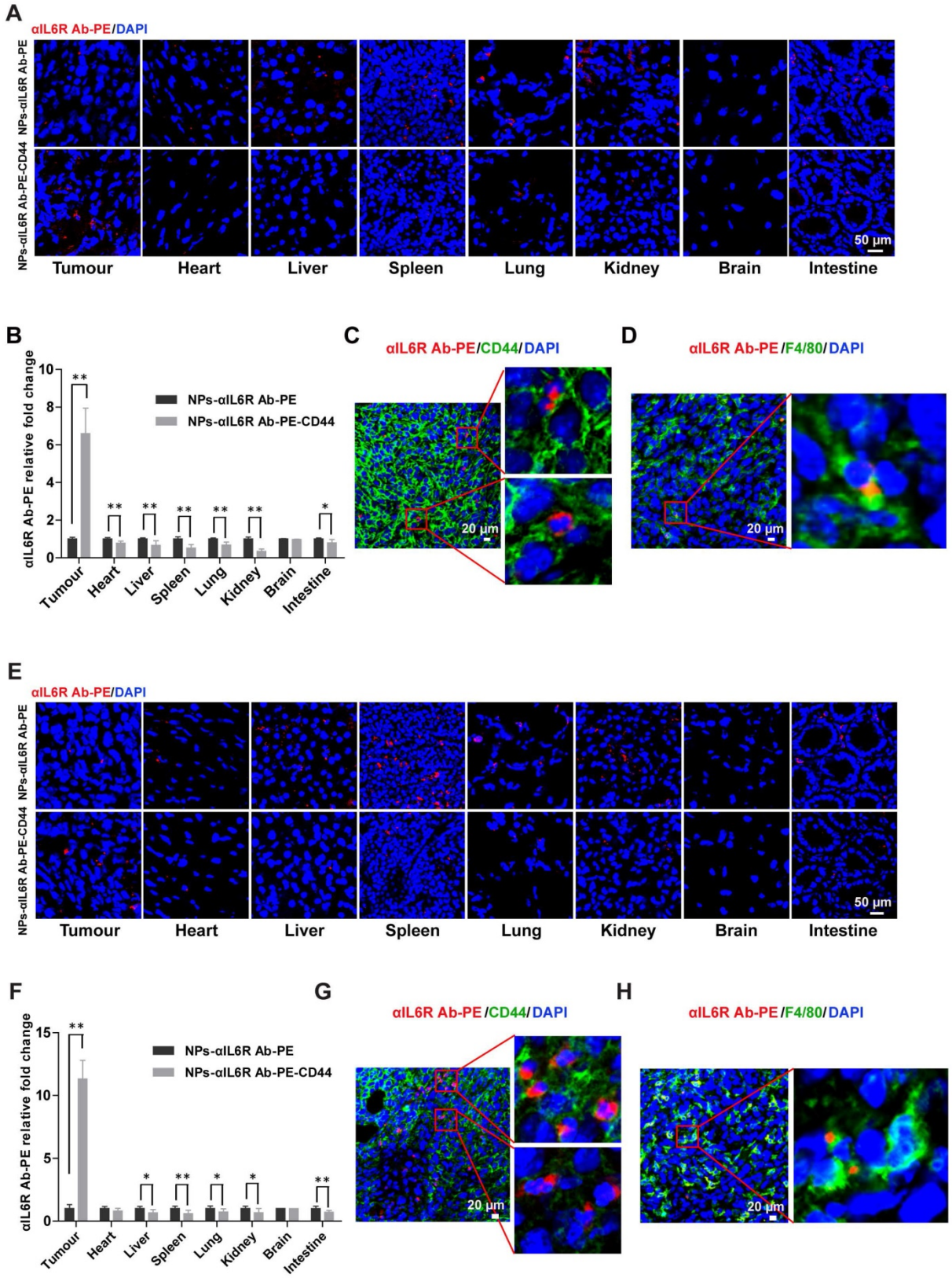

Figure 3. Increased targeting efficiency of CD44 targeted liposomal nanoparticles in breast tumour tissues. **A.** Confocal images of anti-IL6R Ab-PE in various tissues of BALB/c mice bearing 4T1 xenografts that were treated with NPs-αIL6R Ab-PE or NPs-αIL6R Ab-PE-CD44 for 6 hs. **B.** The relative fold changes for the concentration of αIL6R Ab-PE in various tissues of BALB/c mice treated with NPs-αIL6R Ab-PE-CD44 when compared with the NPs-αIL6R Ab-PE treatment control. Data were presented as the mean + SD, n = 6 mice. Representative images showing the distribution of CD44 and anti-IL6R Ab-PE (**C**), F4/80 and anti-IL6R Ab-PE (**D**) in tumour xenografts of BALB/c mice. **E.** Confocal images of anti-IL6R Ab-PE in various tissues of MMTV-PyMT mice. **F.** The relative fold changes for the concentration of anti-IL6R Ab-PE in various tissues of MMTV-PyMT mice treated with NPs-αIL6R Ab-PE-CD44 when compared with the NPs-αIL6R Ab-PE treatment control. Data were presented as the mean + SD, n = 6 mice. The representative images showing the distribution of CD44 and anti-IL6R Ab-PE (**G**), F4/80 and anti-IL6R Ab-PE (**H**) in breast tumours of MMTV-PyMT mice.

Inhibited tumour growth after NPs-αIL6R Ab-CD44 treatment in luminal breast cancer mouse model

To evaluate the therapeutic efficacy of nanoparticles with anti-IL6R antibody *in vivo*, PBS, anti-IL6R Ab, NPs-IgG-CD44, NPs-αIL6R Ab and NPs-αIL6R Ab-CD44 were injected via tail veins into 4T1 tumour-bearing mice (**Figure 4A**) and MMTV-PyMT mice (**Figure 4H**) after tumorigenesis. The treatment was conducted every two days for a total of 3 times. The tumour volumes were monitored at fixed time intervals. As shown in **Figure 4B** and **4I**, although the tumour volume steadily increased in the five groups, tumour growth was slightly reduced in BALB/c mice and significantly retarded in MMTV-PyMT mice injected with NPs-αIL6R Ab-CD44 when compared with the PBS, anti-IL6R Ab, NPs-IgG-CD44 treatment controls. Significantly reduced immunofluorescence staining of BrdU positive cells was observed in both mouse models treated with NPs-αIL6R Ab-CD44 (**Figure 4C** and **4D, Figure 4J** and **4K)** at the time of sacrifice. These findings supported the concept that delivery of anti-IL6R antibody to the TME suppressed tumour growth *in vivo*.

Compromised lung metastasis of breast cancer after NPs-αIL6R Ab-CD44 treatment *in vivo*

To further detect the inhibitory effect of these nanoparticles on tumour metastasis *in vivo*, lung tissues were stained with haematoxylin and eosin (HE) for the identification of metastatic foci (**Figure 4E** and **4L**). Significantly reduced lung metastatic foci number (**Figure 4F** and **4M**) and foci area (**Figure 4G** and **4N**) were found in both mouse models treated with NPs-αIL6R Ab-CD44. This indicated that delivery of anti-IL6R antibody to the TME of $CD44^+$ breast tumour cells could effectively suppress tumour metastasis. The NPs-αIL6R Ab-CD44 possibly performed their effects through multiple sites. It might inhibit the IL6R-Stat3 signaling pathway in tumour cells and simultaneously impede the phenotype transition of macrophage from M1 to M2.

Suppressed production of VEGFA, MMP-9 and reduced M2 macrophages after NPs-αIL6R Ab-CD44 treatment *in vivo*

To test the above hypothesis, the primary tumour tissues and lung metastatic foci were subjected to IHC staining to detect the infiltration of TAMs ($CD206^+$) and the expression level changes of proteins associated with stemness and metastasis. We found that delivery of anti-IL6R antibody to the TME decreased the expression of Stat3, p-Stat3, MMP-9, VEGFA, CD31, Sox2 and CD206 proteins in tumour tissues of 4T1-tumour-bearing mice as well as MMTV-PyMT mice (**Figure 5A** and **5B, Figure 6A** and **6B**). These results demonstrated that NPs-αIL6R Ab-CD44 suppressed the activation of Stat3 and inhibited the expression of its downstream molecules including MMP-9 [26] and Sox2 [32]. In addition, it restrained angiogenesis, as reflected by the reduced expression of VEGFA and the platelet endothelial cell adhesion molecule (CD31). Furthermore, blocking of IL6R signaling inhibited the phenotype conversion of macrophages from M1 to M2, as reflected by the reduced $CD206^+$ cells after NPs-αIL6R Ab-CD44 treatment (**Figure 5A** and **6A**), which formed a tumour microenvironment unfavourable for metastasis. The inhibited expression of Stat3 in tumour tissues upon NPs-αIL6R Ab-CD44 treatment may due to several mechanisms. The reduced TAMs in TME may be one of the key reasons, since TAMs was reported to promote the expression of Stat3 in breast cancer cells through EGF-EGFR signaling pathway [32].

Most importantly, IHC staining of lung tissues disclosed the reduced percentage of $Sox2^+$ tumour cells and $CD206^+$ cells in the metastatic foci (**Figure 5C** and **5D, Figure 6C** and **6D**), indicating that the NPs-αIL6R Ab-CD44 modified the microenvironment of both primary tumour tissues and the lung metastatic foci to repress the lung metastasis of CSCs-like cells *in vivo*.

Discussion

At present, surgery and chemotherapy are the primary treatment methods for breast cancer. However, the clinical effectiveness of systemic therapy is generally compromised by the non-specificity to tumours as well as drug-related toxicity to non-targeted tissues and organs. Furthermore, breast tumour metastasis is among the leading causes of cancer death for female patients. Therefore, methods for improving the efficacy of chemotherapeutic drugs and overcoming tumour metastasis could significantly improve the prognosis of breast cancer patients.

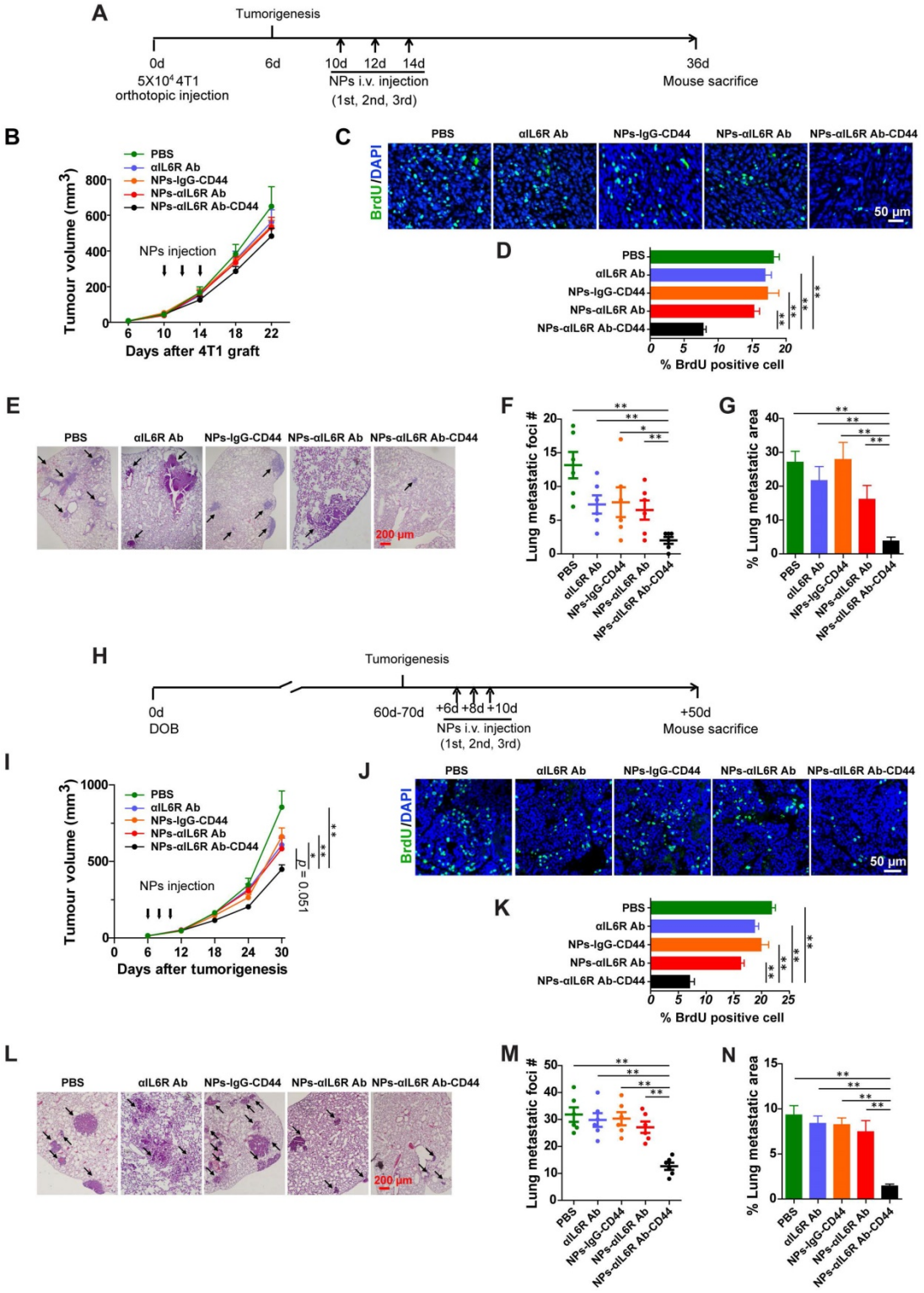

Figure 4. Inhibited tumour metastasis in BALB/c and MMTV-PyMT mice treated with NPs-αIL6R Ab-CD44. **A.** Schematic diagram of the experimental procedure in BALB/c mice. **B.** Growth curve of the 4T1 xenografts in BALB/c mice treated with NPs-αIL6R Ab-CD44 and the controls. Data were presented as the mean + standard error of the mean (SEM, n = 6 mice). **C.** Immunofluorescent staining of BrdU in 4T1 tumour xenografts of BALB/c mice. **D.** Statistics of the percentage of BrdU positive cells in 4T1 tumour xenografts. Data were presented as the mean + SEM, n = 6 mice. **E.** Representative HE staining of metastatic foci in the lung tissues of the BALB/c mice. Statistical results shown for the number (#) of metastatic foci (**F**, data were presented as the mean ± SEM, n = 6 mice) and the relative percentage of metastatic foci area (**G**, data were presented as the mean + SEM, n = 6 mice) in the lung of BALB/c mice. **H.** Schematic diagram of the experimental procedure for MMTV-PyMT mice. DOB, Day of Birth. **I.** Tumour growth curve in the MMTV-PyMT mice treated with NPs-αIL6R Ab-CD44 and the controls, data were presented as the mean + SEM, n = 6 mice Statistical analysis was performed to determine the significance of tumour volume on the 30th days after tumorigenesis. **J.** Immunofluorescent staining of BrdU in tumour tissues of MMTV-PyMT mice. **K.** Statistics of the percentage of BrdU positive cells in tumour tissues of MMTV-PyMT mice treated with NPs-αIL6R Ab-CD44 and the controls, data were presented as the mean + SEM, n = 6 mice. **L.** Representative HE staining of metastatic foci in the lung tissues of MMTV-PyMT mice. Statistical results for the number of metastatic foci (**M**, data were presented as the mean ± SEM, n = 6 mice) and the relative percentage of metastatic foci area (**N**, data were presented as the mean + SEM, n = 6 mice,) in the lung of MMTV-PyMT mice.

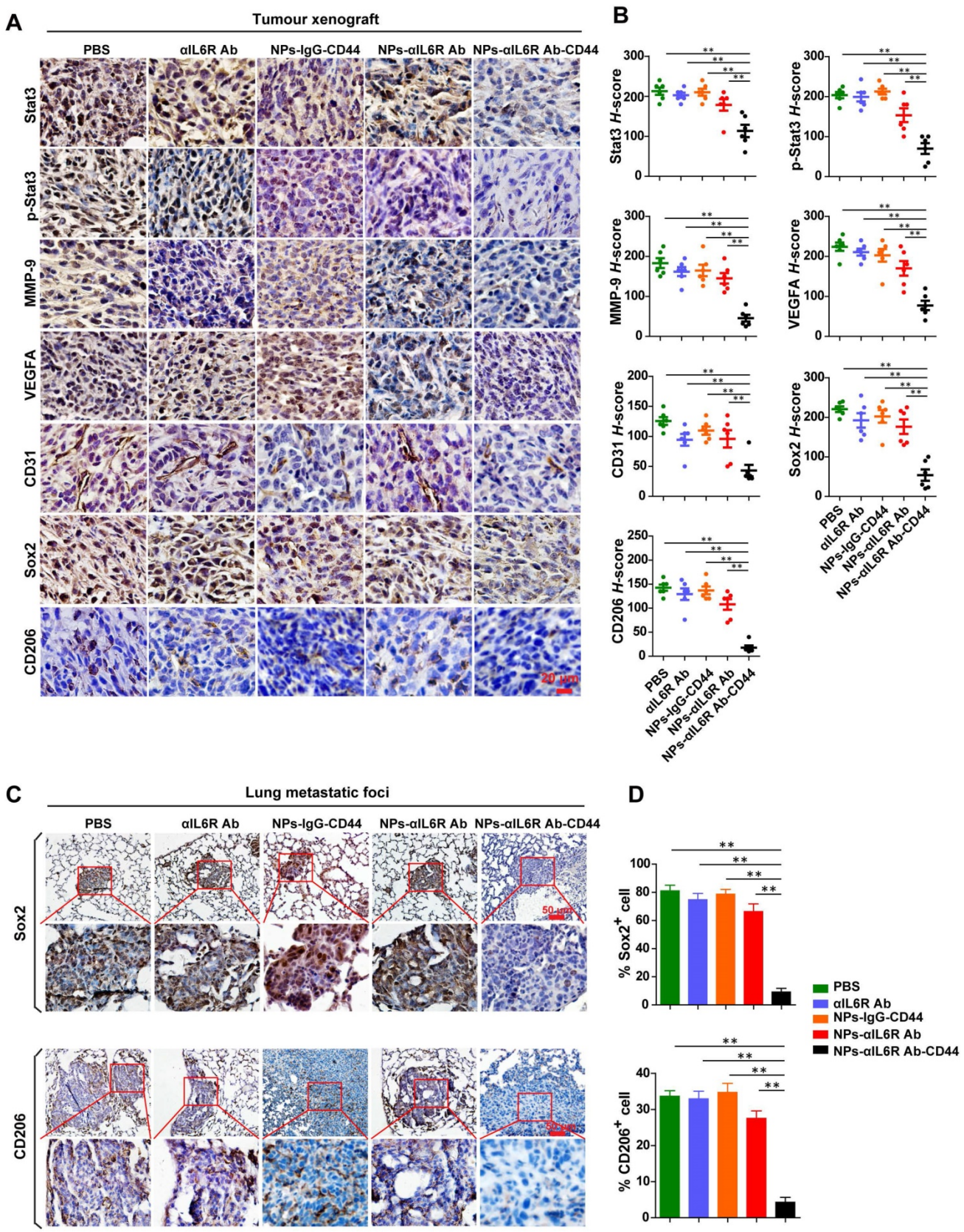

Figure 5. Inhibited IL6R-Stat3 signaling in tumour xenografts and reduced CSCs-like population in lung metastatic foci of BALB/c mice treated with NPs-αIL6R Ab-CD44. **A.** Immunohistochemistry (IHC) staining of Stat3, p-Stat3, MMP-9, VEGFA, CD31, Sox2 and CD206 in 4T1 tumour xenografts from BALB/c mice, which were treated with PBS, anti-IL6R Ab (αIL6R Ab), NPs-IgG-CD44, NPs-αIL6R Ab and NPs-αIL6R Ab-CD44, respectively. **B.** The statistical results of IHC staining for Stat3, p-Stat3, MMP-9, VEGFA, CD31, Sox2 and CD206 of 4T1 tumour xenografts in BALB/c mice. Data were presented as the mean ± SEM, n = 6 mice. **C.** IHC staining of Sox2 and CD206 in the lung metastatic foci. **D.** Statistical analysis for the percentage of $Sox2^+$ and $CD206^+$ cells in the lung metastatic foci. Data were presented as the mean + SEM, n = 6 mice.

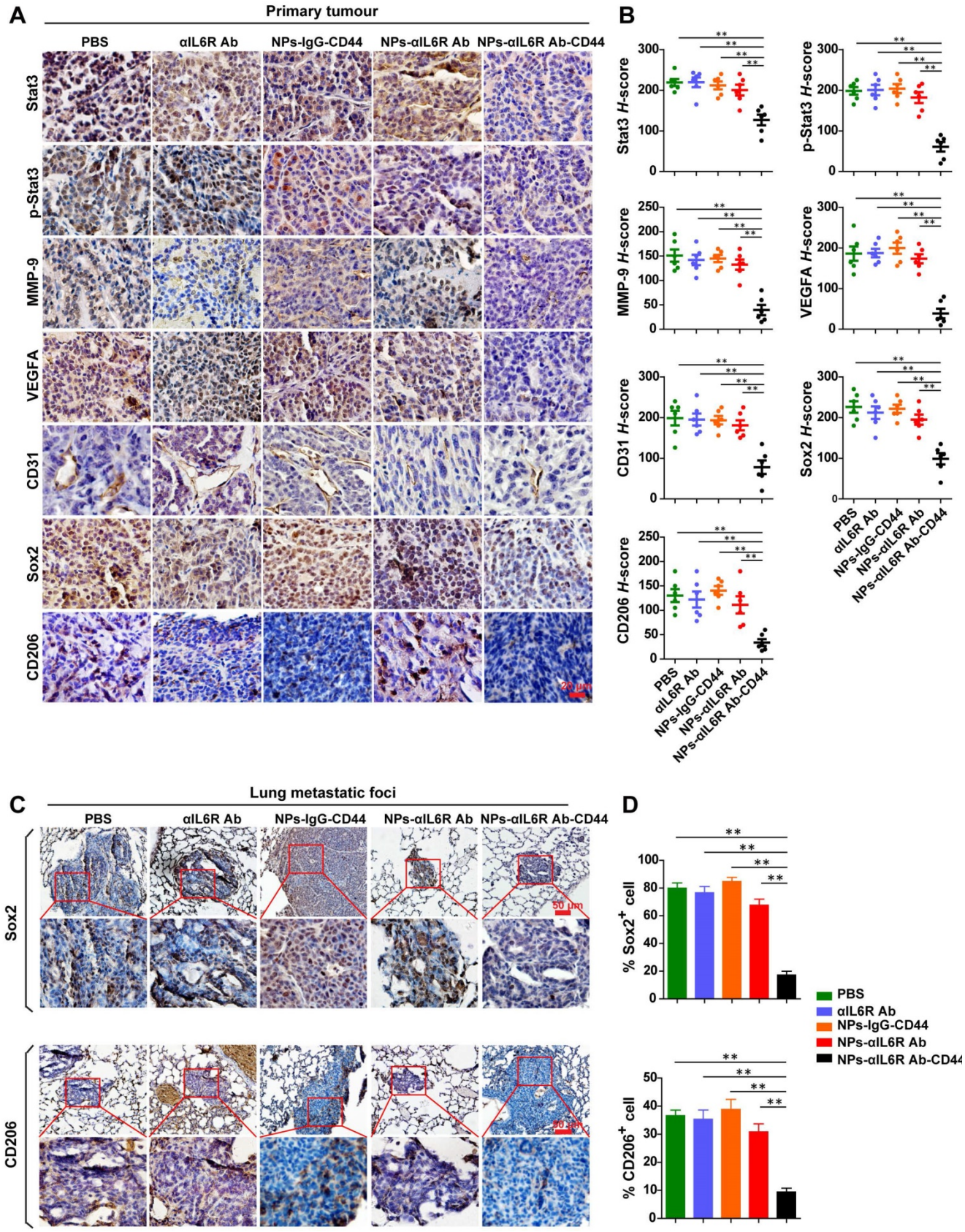

Figure 6. Inhibited IL6R-Stat3 signaling in primary tumour and reduced CSCs-like population in lung metastatic foci of MMTV-PyMT mice treated with NPs-αIL6R Ab-CD44. **A.** IHC staining of Stat3, p-Stat3, MMP-9, VEGFA, CD31, Sox2 and CD206 in primary tumour tissues of MMTV-PyMT mice, which were treated with PBS, αIL6R Ab, NPs-IgG-CD44, NPs-αIL6R Ab and NPs-αIL6R Ab-CD44, respectively. **B.** The statistical results of IHC staining for Stat3, p-Stat3, MMP-9, VEGFA, CD31, Sox2 and CD206 in the primary tumour of MMTV-PyMT mice. Data were presented as the mean ± SEM, n = 6 mice. **C.** IHC staining of Sox2 and CD206 in the lung metastatic foci of MMTV-PyMT mice. **D.** Statistical analysis for the percentage of $Sox2^+$ and $CD206^+$ cells in the lung metastatic foci. Data were presented as mean + SEM, n = 6 mice.

It has been established that various materials can be encapsulated in nanoparticles, such as hemagglutinin-split influenza virus mucosal vaccine encapsulated in chitosan nanoparticles [42], recombinant protein of chlamydia trachomatis sealed in PLGA (poly D, L-lactic-co-glycolic acid) nanoparticles [43], and siRNAs encapsulated in lipid nanoparticles [44]. Meanwhile, liposomes can carry large molecules with therapeutic potential, for example, cDNA, polypeptides as well as small molecules and chemotherapy drugs. In this study, we developed a liposomal nanoparticle that encapsulated anti-IL6R antibody targeting CD44, a transmembrane glycoprotein presented in the breast tumours. This liposomal nanoparticle specifically targeted the TME of $CD44^+$ breast cancer cells, leading to significant inhibition of tumour metastasis and slightly delayed growth of breast tumours. These results are consistent with the numerous reports that IL6R signaling contributed significantly to tumour metastasis [45], and sporadic studies showed its regulatory effect on cell cycle and tumour growth [30, 46]. As continued growth of the primary tumour may eventually lead to metastatic spread, application of this nanoparticle at early tumour stage and combination of this therapy with primary tumour surgery may improve the survival of tumour-bearing mice.

We demonstrated that our liposomal nanoparticles were more efficient in delivering chemicals to solid tumours than the non-targeted liposome. At the same time, the chemical concentrations in major organs and tissues were low, indicating that the systemic side effects of this nanoparticle were minimized. The small size (mean value, 92-121 nm) and narrow PDI of the nanoparticles allowed them to penetrate into the interstitium of tumours through leaky vasculature. In our study, the basic liposomes were composed of DOPC, DOPE, cholesterol and PEG. It was reported that the most pH-sensitive lipid in a DOPC-DOPE liquid phase is DOPE [47]. Thus, pH-sensitive property of NPs-Dox-CD44 or NPs-αIL6R Ab-PE-CD44 could trigger the release of their encapsulated contents into the extracellular matrix based on the difference pH between the tumour extracellular environment and normal tissues. In addition, removal of 1, 2-dioleoyl-3-trimethy-lammonium-propane (DOTAP) from our traditional nanoparticle preparation procedure may enhance the delivery efficacy of anti-IL6R antibody to TME, which can target tumour cells as well as the TAMs and thus promote the anti-tumour effect of anti-IL6R antibody. As can been observed in **Figure S4**, most of the anti-IL6R Ab-PE or Dox did not showed the co-localization with Rab5 and Rab7, which are the marker proteins for the early and late endosome separately, in both tumour models. This phenomenon indicated that our nanoparticle system firstly delivered the loading drugs to the extracellular matrix and reduced the penetration of NPs to cell membrane at the early stage of treatment.

The other important finding from this study was disclosure of the fact that NPs-αIL6R Ab-CD44 suppressed tumour stemness and metastasis *in vivo*. Because Sox2 is the downstream factor of IL6R-Stat3, blocking of IL6R caused down-regulation of Sox2 and inhibition of its stemness-promotion function. Most importantly, we provided the *in vivo* evidence showing that the NPs-αIL6R Ab-CD44 treatment impeded the metastasis of breast cancer in both the 4T1-xenograft mouse model and MMTV-PyMT model through down-regulating the production of cytokines or enzymes such as VEGFA and MMP-9 as well as inhibiting the angiogenesis.

Finally, we demonstrated that the NPs-αIL6R Ab-CD44 specifically modified the immune environment in primary tumour by inhibiting the infiltration of TAMs to form a tumour microenvironment unfavourable for metastasis. It also modified the immune environment of lung metastatic foci, as reflected by the reduced M2 macrophages, which may be one of the key reasons that account for the reduced tumour metastatic area and foci number as well as the CSCs-like $Sox2^+$ population in the lungs metastatic foci.

In summary, our results indicated that the TME targeting nanoparticles loaded with anti-IL6R antibody/chemicals could deliver the drugs effectively to the TME of $CD44^+$ breast tumours. Those nanoparticles inhibited tumour metastasis effectively through blocking the IL6R-Stat3 signaling in tumour cells. They also impeded the infiltration of TAMs both in the 4T1 xenograft, which represented the advanced triple negative breast cancer, and MMTV-PyMT mice, which showed a similar gene expression profile to human luminal breast cancer. This novel nanoparticle thus provided a promising strategy for the clinical treatment of multiple molecular phenotypes of breast cancer by targeting the TME.

Supplementary Material

Supplementary figures.
http://www.thno.org/v07p0775s1.pdf

Acknowledgement

We thank Dr. Ze Liu (School of Medicine, Nankai University, Tianjin, China) for his helpful suggestions for this study.

This work was funded by the Natural Science Foundation of China 81372308 and 81572599 (to N. Li), and China Major national science and technology projects 2013CB967201 (to R. Xiang).

Competing Interests

The authors have declared that no competing interest exists.

References

1. Siegel RL, Miller KD, Jemal A. Cancer statistics, 2016. CA Cancer J Clin. 2016; 66: 7-30.
2. Redig AJ, McAllister SS. Breast cancer as a systemic disease: a view of metastasis. J Intern Med. 2013; 274: 113-126.
3. Bertrand N, Wu J, Xu X, Kamaly N, Farokhzad OC. Cancer nanotechnology: the impact of passive and active targeting in the era of modern cancer biology. Adv Drug Deliv Rev. 2014; 66: 2-25.
4. Mitragotri S, Lahann J. Materials for drug delivery: innovative solutions to address complex biological hurdles. Adv Mater. 2012; 24: 3717-3723.
5. Hamad I, Moghimi SM. Critical issues in site-specific targeting of solid tumours: the carrier, the tumour barriers and the bioavailable drug. Expert Opin Drug Deliv. 2008; 5: 205-219.
6. Cassidy J, Schatzlein AG. Tumour-targeted drug and gene delivery: principles and concepts. Expert Rev Mol Med. 2004; 6: 1-17.
7. Luo D, Carter KA, Lovell JF. Nanomedical engineering: shaping future nanomedicines. Wiley Interdiscip Rev Nanomed Nanobiotechnol. 2015; 7: 169-188.
8. Papahadjopoulos D, Allen TM, Gabizon A, Mayhew E, Matthay K, Huang SK, et al. Sterically stabilized liposomes: improvements in pharmacokinetics and antitumor therapeutic efficacy. Proc Natl Acad Sci U S A. 1991; 88: 11460-11464.
9. Gao Y, Xie J, Chen H, Gu S, Zhao R, Shao J, et al. Nanotechnology-based intelligent drug design for cancer metastasis treatment. Biotechnol Adv. 2014; 32: 761-777.
10. Drummond DC, Zignani M, Leroux J. Current status of pH-sensitive liposomes in drug delivery. Prog Lipid Res. 2000; 39: 409-460.
11. Felber AE, Dufresne MH, Leroux JC. pH-sensitive vesicles, polymeric micelles, and nanospheres prepared with polycarboxylates. Adv Drug Deliv Rev. 2012; 64: 979-992.
12. Park SM, Kim MS, Park SJ, Park ES, Choi KS, Kim YS, et al. Novel temperature-triggered liposome with high stability: formulation, in vitro evaluation, and in vivo study combined with high-intensity focused ultrasound (HIFU). J Control Release. 2013; 170: 373-379.
13. de la Rica R, Aili D, Stevens MM. Enzyme-responsive nanoparticles for drug release and diagnostics. Adv Drug Deliv Rev. 2012; 64: 967-978.
14. Carter KA, Shao S, Hoopes MI, Luo D, Ahsan B, Grigoryants VM, et al. Porphyrin-phospholipid liposomes permeabilized by near-infrared light. Nat Commun. 2014; 5: 3546.
15. Podaru G, Ogden S, Baxter A, Shrestha T, Ren S, Thapa P, et al. Pulsed magnetic field induced fast drug release from magneto liposomes via ultrasound generation. J Phys Chem B. 2014; 118: 11715-11722.
16. Al-Hajj M, Wicha MS, Benito-Hernandez A, Morrison SJ, Clarke MF. Prospective identification of tumorigenic breast cancer cells. Proc Natl Acad Sci U S A. 2003; 100: 3983-3988.
17. Collins AT, Berry PA, Hyde C, Stower MJ, Maitland NJ. Prospective identification of tumorigenic prostate cancer stem cells. Cancer Res. 2005; 65: 10946-10951.
18. Dalerba P, Dylla SJ, Park IK, Liu R, Wang X, Cho RW, et al. Phenotypic characterization of human colorectal cancer stem cells. Proc Natl Acad Sci U S A. 2007; 104: 10158-10163.
19. Wang L, Su W, Liu Z, Zhou M, Chen S, Chen Y, et al. CD44 antibody-targeted liposomal nanoparticles for molecular imaging and therapy of hepatocellular carcinoma. Biomaterials. 2012; 33: 5107-5114.
20. Vinogradov S, Wei X. Cancer stem cells and drug resistance: the potential of nanomedicine. Nanomedicine (Lond). 2012; 7: 597-615.
21. Weber CE, Kuo PC. The tumor microenvironment. Surg Oncol. 2012; 21: 172-177.
22. Ungefroren H, Sebens S, Seidl D, Lehnert H, Hass R. Interaction of tumor cells with the microenvironment. Cell Commun Signal. 2011; 9: 18.
23. Gil-Bernabe AM, Ferjancic S, Tlalka M, Zhao L, Allen PD, Im JH, et al. Recruitment of monocytes/macrophages by tissue factor-mediated coagulation is essential for metastatic cell survival and premetastatic niche establishment in mice. Blood. 2012; 119: 3164-3175.
24. Kaplan RN, Rafii S, Lyden D. Preparing the "soil": the premetastatic niche. Cancer Res. 2006; 66: 11089-11093.
25. Zhao G, Zhu G, Huang Y, Zheng W, Hua J, Yang S, et al. IL-6 mediates the signal pathway of JAK-STAT3-VEGF-C promoting growth, invasion and lymphangiogenesis in gastric cancer. Oncol Rep. 2016; 35: 1787-1795.
26. Ko HS, Park BJ, Choi SK, Kang HK, Kim A, Kim HS, et al. STAT3 and ERK Signaling Pathways Are Implicated in the Invasion Activity by Oncostatin M through Induction of Matrix Metalloproteinases 2 and 9. Yonsei Med J. 2016; 57: 761-768.
27. Zou M, Zhang X, Xu C. IL6-induced metastasis modulators p-STAT3, MMP-2 and MMP-9 are targets of 3,3'-diindolylmethane in ovarian cancer cells. Cell Oncol (Dordr). 2016; 39: 47-57.
28. Guryanova OA, Wu Q, Cheng L, Lathia JD, Huang Z, Yang J, et al. Nonreceptor tyrosine kinase BMX maintains self-renewal and tumorigenic potential of glioblastoma stem cells by activating STAT3. Cancer Cell. 2011; 19: 498-511.
29. Iliopoulos D, Hirsch HA, Wang G, Struhl K. Inducible formation of breast cancer stem cells and their dynamic equilibrium with non-stem cancer cells via IL6 secretion. Proc Natl Acad Sci U S A. 2011; 108: 1397-1402.
30. Wang H, Lathia JD, Wu Q, Wang J, Li Z, Heddleston JM, et al. Targeting interleukin 6 signaling suppresses glioma stem cell survival and tumor growth. Stem Cells. 2009; 27: 2393-2404.
31. Wang Q, Ni H, Lan L, Wei X, Xiang R, Wang Y. Fra-1 protooncogene regulates IL-6 expression in macrophages and promotes the generation of M2d macrophages. Cell Res. 2010; 20: 701-712.
32. Yang J, Liao D, Chen C, Liu Y, Chuang TH, Xiang R, et al. Tumor-associated macrophages regulate murine breast cancer stem cells through a novel paracrine EGFR/Stat3/Sox-2 signaling pathway. Stem Cells. 2013; 31: 248-258.
33. Mou W, Xu Y, Ye Y, Chen S, Li X, Gong K, et al. Expression of Sox2 in breast cancer cells promotes the recruitment of M2 macrophages to tumor microenvironment. Cancer Lett. 2015; 358: 115-123.
34. Hwang SY, Kim HK, Choo J, Seong GH, Hien TB, Lee EK. Effects of operating parameters on the efficiency of liposomal encapsulation of enzymes. Colloids Surf B Biointerfaces. 2012; 94: 296-303.
35. Arabi L, Badiee A, Mosaffa F, Jaafari MR. Targeting CD44 expressing cancer cells with anti-CD44 monoclonal antibody improves cellular uptake and antitumor efficacy of liposomal doxorubicin. J Control Release. 2015; 220: 275-286.
36. Niu C, Wang Z, Lu G, Krupka TM, Sun Y, You Y, et al. Doxorubicin loaded superparamagnetic PLGA-iron oxide multifunctional microbubbles for dual-mode US/MR imaging and therapy of metastasis in lymph nodes. Biomaterials. 2013; 34: 2307-2317.
37. Xu Y, Zhang S, Niu H, Ye Y, Hu F, Chen S, et al. STIM1 accelerates cell senescence in a remodeled microenvironment but enhances the epithelial-to-mesenchymal transition in prostate cancer. Sci Rep. 2015; 5: 11754.
38. Tao K, Fang M, Alroy J, Sahagian GG. Imagable 4T1 model for the study of late stage breast cancer. BMC Cancer. 2008; 8: 228.
39. Kaur P, Nagaraja GM, Zheng H, Gizachew D, Galukande M, Krishnan S, et al. A mouse model for triple-negative breast cancer tumor-initiating cells (TNBC-TICs) exhibits similar aggressive phenotype to the human disease. BMC Cancer. 2012; 12: 120.
40. Kim IS, Baek SH. Mouse models for breast cancer metastasis. Biochem Biophys Res Commun. 2010; 394: 443-447.
41. Vargo-Gogola T, Rosen JM. Modelling breast cancer: one size does not fit all. Nat Rev Cancer. 2007; 7: 659-672.
42. Sawaengsak C, Mori Y, Yamanishi K, Mitrevej A, Sinchaipanid N. Chitosan nanoparticle encapsulated hemagglutinin-split influenza virus mucosal vaccine. AAPS PharmSciTech. 2014; 15: 317-325.
43. Fairley SJ, Singh SR, Yilma AN, Waffo AB, Subbarayan P, Dixit S, et al. Chlamydia trachomatis recombinant MOMP encapsulated in PLGA nanoparticles triggers primarily T helper 1 cellular and antibody immune responses in mice: a desirable candidate nanovaccine. Int J Nanomedicine. 2013; 8: 2085-2099.
44. Katakowski JA, Mukherjee G, Wilner SE, Maier KE, Harrison MT, DiLorenzo TP, et al. Delivery of siRNAs to Dendritic Cells Using DEC205-Targeted Lipid Nanoparticles to Inhibit Immune Responses. Mol Ther. 2016; 24: 146-155.
45. Rokavec M, Oner MG, Li H, Jackstadt R, Jiang L, Lodygin D, et al. IL-6R/STAT3/miR-34a feedback loop promotes EMT-mediated colorectal cancer invasion and metastasis. J Clin Invest. 2014; 124: 1853-1867.
46. Liu D, Liu C, Wang X, Ingvarsson S, Chen H. MicroRNA-451 suppresses tumor cell growth by down-regulating IL6R gene expression. Cancer Epidemiol. 2014; 38: 85-92.
47. Chakraborty H, Sengupta T, Lentz BR. pH Alters PEG-mediated fusion of phosphatidylethanolamine-containing vesicles. Biophys J. 2014; 107: 1327-1338.